Oxygen Transport Ceramic Membranes

Quarterly Report

October 2004 – December 2004

Principal Authors:

Prof. S. Bandopadhyay

Dr. N. Nagabhushana

Dr. T. Nithyanantham

Issued: February 2005

DOE Award # DE-FC26-99FT40054

University of Alaska Fairbanks
Fairbanks, AK 99775

Contributing sub contractors:

1. **X.-D Zhou, Y-W. Sin and H. U. Anderson,** Materials Research Center, University of Missouri-Rolla, Rolla, MO 65401
2. **Prof. Alan Jacobson and Prof. C.A. Mims;** University of Houston/University of Toronto

DISCLAIMER

ABSTRACT

The present quarterly report describes some of the investigations on the structural properties of dense OTM bars provided by Praxair and studies on newer composition of Ti doped LSF.

Thermogravimetric analysis (TGA) was carried out on $La_{0.2}Sr_{0.8}Fe_{0.55}Ti_{0.45}O_{3-\delta}$ to investigate oxygen deficiency (δ) of the sample. The TGA was performed in a controlled atmosphere using oxygen, argon, carbon monoxide and carbon dioxide with adjustable gas flow rates. In this experiment, the weight loss and gain of $La_{0.2}Sr_{0.8}Fe_{0.55}Ti_{0.45}O_{3-\delta}$ was directly measured by TGA. The weight change of the sample was evaluated at between 600 and 1250^{o}C in air or 1000^{o}C as a function of oxygen partial pressure. The oxygen deficiencies calculated from TGA data as a function of oxygen activity and temperature will be estimated and compared with that from neutron diffraction measurement in air.

The LSFT and LSFT/CGO membranes were fabricated from the powder obtained from Praxair Specialty Ceramics. The sintered membranes were subjected to microstructure analysis and hardness analysis. The LSFT membrane is composed of fine grains with two kinds of grain morphology. The gain size distribution was characterized using image analysis. In LSFT/CGO membrane a lot of grain pullout was observed from the less dense, porous phase. The hardness of the LSFT and dual phase membranes were studied at various loads. The hardness values obtained from the cross section of the membranes were also compared to that of the values obtained from the surface.

An electrochemical cell has been designed and built for measurements of the Seebeck coefficient as a function of temperature and pressure. Measurements on $La_{0.2}Sr_{0.8}Fe_{0.55}Ti_{0.45}O_{3-\delta}$ as a function of temperature an oxygen partial pressure are reported. Further analysis of the dilatometry data obtained previously is presented. A series of isotope transients under air separation mode (small gradient) were completed on the membrane of LSCrF-2828 at 900°C. Low pO_2 atmospheres based on with CO - CO_2 mixtures have also been admitted to the delivery side of the LSCrF-2828 membrane to produce the gradients which exist under syngas generation conditions. The CO - CO_2 mixtures have normal isotopic ^{18}O abundances. The evolution of ^{18}O on the delivery side in these experiments after an ^{18}O pulse on the air side reveals a wealth of information about the oxygen transport processes.

TABLE OF CONTENTS

LIST OF GRAPHICAL MATERIALS

INTRODUCTION

Conversion of natural gas to liquid fuels and chemicals is a major goal for the Nation as it enters the 21st Century. Technically robust and economically viable processes are needed to capture the value of the vast reserves of natural gas on Alaska's North Slope, and wean the Nation from dependence on foreign petroleum sources. Technologies that are emerging to fulfill this need are all based syngas as an intermediate. Syngas (a mixture of hydrogen and carbon monoxide) is a fundamental building block from which chemicals and fuels can be derived. Lower cost syngas translates directly into more cost-competitive fuels and chemicals.

The currently practiced commercial technology for making syngas is either steam methane reforming (SMR) or a two-step process involving cryogenic oxygen separation followed by natural gas partial oxidation (POX). These high-energy, capital-intensive processes do not always produce syngas at a cost that makes its derivatives competitive with current petroleum-based fuels and chemicals.

In the mid 80's BP invented a radically new technology concept that will have a major economic and energy efficiency impact on the conversion of natural gas to liquid fuels, hydrogen, and chemicals.[1] This technology, called Electropox, integrates oxygen separation with the oxidation and steam reforming of natural gas into a single process to produce syngas with an economic advantage of 30 to 50 percent over conventional technologies.[2]

The Electropox process uses novel and proprietary solid metal oxide ceramic oxygen transport membranes [OTMs], which selectively conduct both oxide ions and electrons through their lattice structure at elevated temperatures.[3] Under the influence of an oxygen partial pressure gradient, oxygen ions move through the dense, nonporous membrane lattice at high rates with

---

[1]Mazanec, T. J.; Cable, T. L.; Frye, J. G., Jr.; US 4,793,904, 27 Dec **1988**, assigned to The Standard Oil Company (now BP America), Mazanec, T. J.; Cable, T. L.; US 4,802,958, 7 Feb **1989**, assigned to the Standard Oil Co. (now BP America), Cable, T. L.; Mazanec, T. J.; Frye, J. G., Jr.; European Patent Application 0399833, 24 May **1990**, published 28 November **1990.**

[2]Bredesen, R.; Sogge, J.; "A Technical and Economic Assessment of Membrane Reactors for Hydrogen and Syngas Production" presented at Seminar on the Ecol. Applic. of Innovative Membrane Technology in the Chemical Industry", Cetraro, Calabria, Italy, 1-4 May **1996**.

[3]Mazanec, T.J., *Interface*, **1996**; Mazanec, T.J., *Solid State Ionics*, 70/71, **1994** 11-19; "Electropox: BP's Novel Oxidation Technology", T.J. Mazanec, pp 212-225, in "The Role of Oxygen in Improving Chemical Processes", M. Fetizon and W.J. Thomas, eds, Royal Society of Chemistry, London, **1993**; "Electropox: BP's Novel Oxidation Technology", T.J. Mazanec, pp 85-96, in "The Activation of Dioxygen and Homogeneous Catalytic Oxidation", D.H.R. Barton, A. E. Martell, D.T. Sawyer, eds, Plenum Press, New York, **1993**; "Electrocatalytic Cells for Chemical Reaction", T.J. Mazanec, T.L. Cable, J.G. Frye, Jr.; Prep Petrol Div ACS, San Fran, **1992** *37*, 135-146; T.J. Mazanec, T.L. Cable, J.G. Frye, Jr.; *Solid State Ionics*, **1992**, 53-56, 111-118.

100 percent selectivity. Transported oxygen reacts with natural gas on the fuel side of the ceramic membrane in the presence of a catalyst to produce syngas.

In 1997 BP entered into an OTM Alliance with Praxair, Amoco, Statoil and Sasol to advance the Electropox technology in an industrially sponsored development program. These five companies have been joined by Phillips Petroleum and now are carrying out a multi-year $40+ million program to develop and commercialize the technology. The program targets materials, manufacturing and engineering development issues and culminates in the operation of semi-works and demonstration scale prototype units.

The Electropox process represents a truly revolutionary technology for conversion of natural gas to synthesis gas not only because it combines the three separate unit operations of oxygen separation, methane oxidation and methane steam reforming into a single step, but also because it employs a chemically active ceramic material in a fundamentally new way. On numerous fronts the commercialization of Electropox demands solutions to problems that have never before been accomplished. Basic problems in materials and catalysts, membrane fabrication, model development, and reactor engineering all need solutions to achieve commercial success.

Six important issues have been selected as needing understanding on a fundamental level at which the applied Alliance program cannot achieve the breadth and depth of understanding needed for rapid advancement. These issues include:

1. Oxygen diffusion kinetics (University of Houston);
2. Phase stability and stress development (University of Missouri - Rolla);
3. Mechanical property evaluation in thermal and chemical stress fields (University of Alaska Fairbanks)

Statement of Work

Task 1 *Evaluate phase stability and thermal expansion of candidate perovskite membranes and develop techniques to support these materials on porous metal structures.*

Task 2 *Determine materials mechanical properties under conditions of high temperatures and reactive atmospheres.*

Task 3 *Measure kinetics of oxygen uptake and transport in ceramic membrane materials under commercially relevant conditions using isotope labeling techniques.*

EXECUTIVE SUMMARY

Research on the Oxygen Transport Membranes as listed as tasks 1-3 are being performed at the various universities under the stewardship of Praxair. The quarterly technical report presents the progress of the tasks defined to understand the fundamental concepts and structural performance of the OTM material.

Thermogravimetric analysis (TGA) was carried out on $La_{0.2}Sr_{0.8}Fe_{0.55}Ti_{0.45}O_{3-\delta}$ to investigate oxygen deficiency (δ) of the sample at 600 and 1250^{o}C in air or 1000^{o}C as a function of oxygen partial pressure. The oxygen deficiencies calculated from TGA data as a function of oxygen activity and temperature were estimated and compared with that from neutron diffraction measurement in air. The calculated oxygen deficiencies from the weight loss from air to PO_2 = 1.45E-14 is about 0.034 moles of oxygen at 1000^{o}C. In the previous report, the oxygen occupancy (3-δ) calculated from the neutron diffraction data is 2.95 at 800^{o}C in air. Although more investigation is necessary to determine oxygen occupancy at a certain temperature, 2.95 at 800^{o}C was chosen to be the reference point based on the current data to determine the oxygen occupancies at higher than 800^{o}C. Therefore the oxygen occupancies at 1000^{o}C were estimated from the reference point at 800^{o}C from neutron diffraction and the data from the TGA analysis between 800 and 1000^{o}C and it was about 2.94 in air. Using the above estimation, the oxygen occupancies in PO_2 = 1.45E-14 at 1000^{o}C is 2.90. On the other hand, a discrepancy in the data is observed in that the weight gain at $PO_2 = 1 \times 10^{-10}$ when PO_2 was decreased and it was not observed when PO_2 was increased. More investigation about this PO_2 region will be required to clarify this problem.

Dense single phase $La_{0.2}Sr_{0.8}Fe_{0.6}Ti_{0.4}O_{3-\delta}$ and dual phase $La_{0.2}Sr_{0.8}Fe_{0.6}Ti_{0.4}O_{3-\delta}$/CGO OTM bars were fabricated at Praxair research facilities. The OTM bars were analyzed for microstructure at UAF. The hardness were measured and a maximum hardness of 6.0 GPa for LSFT and 6.2 GPa for dual phase membrane was observed. In LSFT, the scatter in hardness values decreased with increasing load which confirms the uniform distribution of pores in the membrane. In the dual phase membrane this behavior, however, was not observed. In both the materials, in comparison the hardness at the cross section was slightly inferior to that of the surface hardness.

University of Houston and University of Toronto have continued to investigate the thermodynamic properties (stability and phase-separation behaviour) and total conductivity of prototype membrane materials. The data are needed together with the kinetic information to develop a complete model for the membrane transport. We have previously reported characterization, stoichiometry, conductivity, and dilatometry measurements for samples of $La_{0.2}Sr_{0.8}Fe_{0.55}Ti_{0.45}O_{3-x}$. In this period, we have measurements of the Seebeck coefficient and report the results. We have also analyzed the thermal

expansion data in more detail to reveal the variation of the thermal expansion coefficient as a function of temperature. On heating, the expansion coefficient reaches a maximum value of ~ 12×10^{-6} K^{-1} and then falls to ~ 10×10^{-6} K^{-1} at 550 °C. Above 750 °C, the expansion coefficient drops smoothly to ~ 8×10^{-6} K^{-1} at 1100 °C. The average TEC of $La_{0.2}Sr_{0.8}Fe_{0.55}Ti_{0.45}O_{3-\delta}$ over the whole temperature range is $9.3 \pm 1.1 \times 10^{-6}$ K^{-1}. The chemical expansion data are consistent with the previous stoichiometry and conductivity observations on this material and on other ferrites that all show very slow kinetics in the intermediate pressure range. The data suggest some non-equilibrium behavior which is most likely associated with cation diffusion or rearrangement of microdomains.

In the area of isotope transient studies at steady state, the current quarter has been dominated by continued analysis of the data from the isotope transients and the analysis of the profile in the quenched membrane. Air separation transients were fit to the 1-D transport model. The oxygen diffusivity did not show a significant dependence on the average oxygen activity in the membrane over the modest range used. The derived values of the forward oxygen surface activation rate coefficient for the same transients were obtained as function of the air-side oxygen partial pressure. Some variability with the value of the oxygen partial pressure on the delivery side was observed but the expected systematic variation, showing higher forward rate coefficients with increasing gradient across the membrane was not evident in the data. In a high gradient experiment molecular oxygen appeared on the sweep side of the membrane indicating that oxygen recombination was sufficiently fast to compete with CO oxidation for oxygen. The activity gradient in the membrane was therefore modest and similar to the air separation experiments. When the gas admitted was 50% CO, the membrane switched to high gradient – high flux mode. The time scale is much shorter, in agreement with the substantially higher oxygen flux and no molecular oxygen is seen. If the entire delivery surface is at sufficient low oxygen potential, molecular oxygen formation is thermodynamically prohibited, consistent with our observations.

Task 1: Preparation and Characterization of Dense Ceramic oxygen Permeable Membranes

X.-D Zhou[1], Q. Cai[2], J. Yang[1], W. B. Yelon[1], W. J. James[1] and H. U. Anderson[1]

1. **Materials Research Center, University of Missouri-Rolla, Rolla, MO 65401**
2. **Department of Physics, University of Missouri-Columbia, Columbia, MO 65211**

Thermogravimetric analysis of $La_{0.2}Sr_{0.8}Fe_{0.55}Ti_{0.45}O_{3-\delta}$ as a function of PO_2 at elevated temperatures

Experimental

The thermogravimetic apparatus used in the current experiment is a Cahn balance (Model TG-171) which is located in the Electronic Materials Applied Research Center in University of Missouri - Rolla. The reliable accuracy limit of Cahn balance in UMR is approximately ±0.4 milligrams or $\pm 7.5 \times 10^{-4}$ moles oxygen even though the minimum detection limit is ±1 micro gram or $\pm 1.8 \times 10^{-6}$ moles oxygen for $La_{0.2}Sr_{0.8}Fe_{0.55}Ti_{0.45}O_{3-\delta}$ (LSFT). The TGA consists of a balance from which up to 100 grams of sample can be suspended in a vertical furnace that is sealed from the atmosphere. The atmosphere is controlled by using different gases such as oxygen, air, argon, carbon monoxide and carbon dioxide. The gas flow rate is also controlled by using MFC (mass flow controller by MKS and Tylan General) and MKS 244A multi-channel analog controller and Tylan controller. A personal computer and TGA operation program from Cahn controls temperature schedule and collect data for weight change and draw plots as a function of time.

In the current experiment, the 5 grams of powder sample of $La_{0.2}Sr_{0.8}Fe_{0.55}Ti_{0.45}O_{3-\delta}$ was used for thermogravimetic measurement. The same sample was used for all the experiments in this report. Carbon monoxide and carbon dioxide gases were mixed with a certain ratio in a gas mixing apparatus to produce the desired oxygen activity and flowed into the furnace tube.

The gas flow rate of 0.2 cm/sec of was used to minimize the buoyancy effect caused by the positive gas pressure due to the gas flow from the bottom of the alumina

tube which is vertically mounted in the TGA furnace system. The powder sample was placed into the alumina bucket which was suspended inside of the vertical furnace tube using sapphire wire whose the other end is attached to the balance which is located on the top of the TGA apparatus. The CO and CO_2 gases were separately delivered from their cylinders at a certain flow rate into a gas mixing chamber which is filled with hundreds of small hallow glass tubes (the length of glass tube is about 0.5 ~ 1 cm) and were thoroughly mixed with argon in the same gas mixing chamber to dilute the CO/CO_2 gas mixture before entering the furnace tube. The dilution ratio of CO/CO_2 mixture and argon is 10% / 90%. The reason of this process is that the dilution with argon could minimize the modification of CO/CO_2 ratio caused by thermal diffusion or thermal gradient inside of furnace tube in high temperatures. The oxygen activities were monitored by using a zirconia oxygen sensor in a separate furnace. Air was used as the reference gas. The relationship for oxygen activity is

$$E_v = -\frac{RT}{4F}\ln\frac{PO_2^{'}}{PO_2^{''}}$$

where $PO_2^{'}$ and $PO_2^{''}$ are the oxygen activity in the measuring cell and in air, and T_k is the absolute temperature of the specimen.

The details oxygen partial pressures calculated thermodynamically are described in Table I.

Table I. The oxygen partial pressure used in this experiment at 1000°C

	E_v	PO_2 at 1000°C
Air		0.21
0.01% O_2 – Balance Ar	0.187	1.19E-4
CO/CO_2	0.690	2.48E-12
CO/CO_2	0.771	1.29E-13
CO/CO_2	0.831	1.45E-14

Results and Discussion

The initial weight was stabilized after several hours at room temperature in air, before the TGA program was started, and additional 2 hours was added after TGA program was started, and then the TGA furnace was actually heated up to high temperatures. The starting weight was achieved during that last two hours and it was recorded as shown in Figures 1 and 2. The starting weight was compared with the ending weight to see if any irreversible weight change had occurred. Before starting the TGA measurement, the sample was calcined in air in the furnace at 1250°C for 5 hours in order to minimize volatile organics. After this high temperature calcination process, the sample was annealed at 1000 and 1200°C in air, respectively, to see if the sample weight was fully reversible. (Figure 1 and 2)

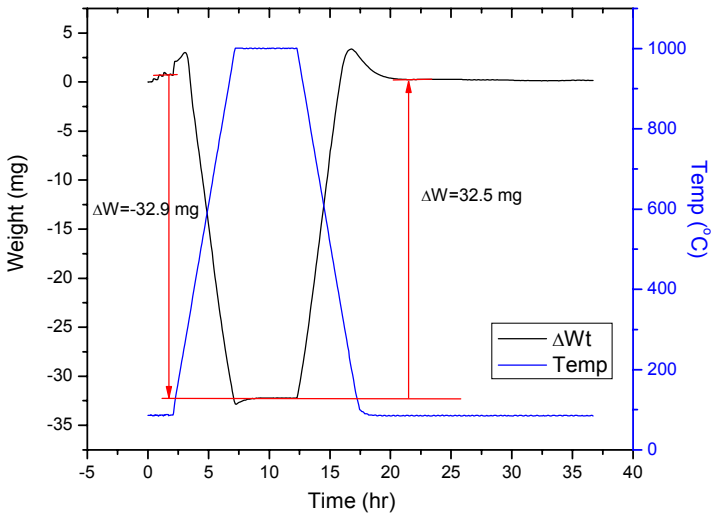

Figure 1. The weight change during annealing of $La_{0.2}Sr_{0.8}Fe_{0.55}Ti_{0.45}O_{3-\delta}$ measured by TGA at 1000°C in Air

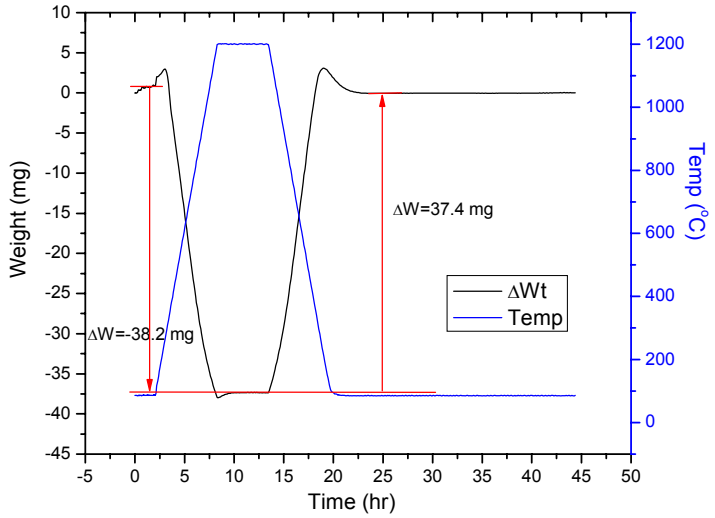

Figure 2. The weight change during annealing of $La_{0.2}Sr_{0.8}Fe_{0.55}Ti_{0.45}O_{3-\delta}$ measured by TGA at 1200°C in Air

The weight loss of LSFT during heating up to 1000°C was about 32.9 mg while the weight gain during cooling down to room temperature was 32.5 mg (shown in Figure 1). The weight loss up to 1200°C was about 38.2 mg while the weight gain down to room temperature was 37.4 mg (shown in Figure 2). The difference between weight loss and gain at 1000°C was 0.4 mg and that at 1200°C was 0.8 mg. These numbers were within the reliable accuracy limit of TGA so that the sample was considered to be fully reversible. The full reversibility ensured that oxygen was the only volatile component of the LSFT powder sample. The difference of total weight loss during heating between 1000 and 1200°C was 5.3 mg which indicated that 0.01 moles of more oxygen was lost from the LSFT sample as it was heated from 1000°C to 1200°C. The evaluation of weight change is important because it is used to determine oxygen deficiency of LSFT as a function of temperature and/or PO_2. The results for weight loss and corresponding oxygen deficiency of LSFT as a function of temperature are shown in Figure 3.

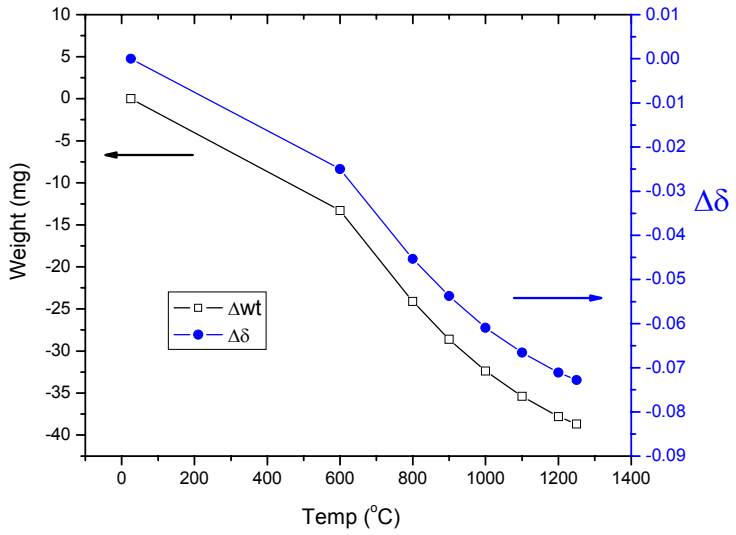

Figure 3. The weight loss and oxygen deficiency from room temperature to 1250°C of $La_{0.2}Sr_{0.8}Fe_{0.55}Ti_{0.45}O_{3-\delta}$ measured by TGA as a function of PO_2

Since there was no reference at a certain temperature, zero weight change was assigned at room temperature as a reference point where assumes full oxygen stoichiometry. Therefore, only absolute weight changes were evaluated at higher temperatures and only relative oxygen deficiencies could be determined as a function of temperature. In the previous report, oxygen occupancies were evaluated using neutron diffraction analysis in air as a function of temperature and the oxygen occupancies from room temperature up to 900°C were determined. However, when the absolute oxygen deficiency was compared between neutron diffraction analysis and TGA analysis, it was found that there were discrepancies in oxygen deficiency which is shown in Figure 4. The trend of oxygen deficiency in neutron diffraction analysis between 100 and 800°C was roughly matched with that in TGA analysis. However, there were huge discrepancies of the oxygen deficiency at room temperature and 900°C. Therefore the further study is suggested to investigate discrepancies between the neutron diffraction data and TGA data.

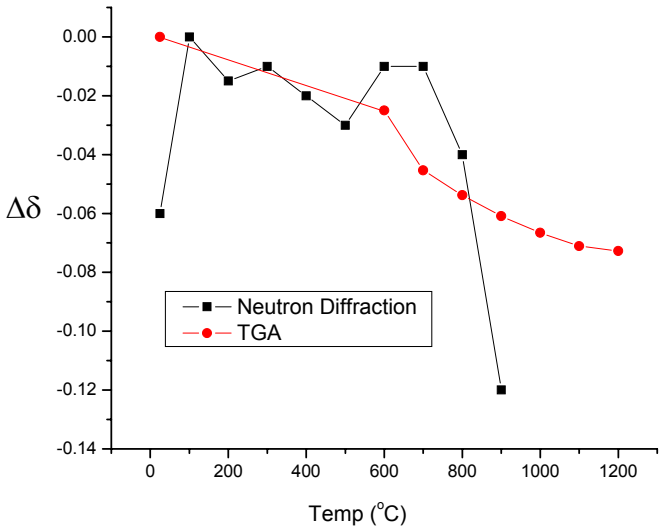

Figure 4. The oxygen deficiency of LSFT from neutron diffraction analysis and TGA analysis as a function of temperature

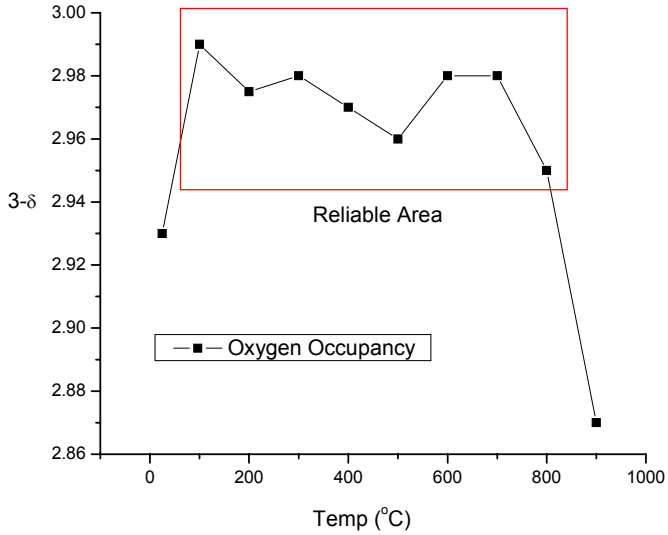

Figure 5. The oxygen occupancy of LSFT from neutron diffraction analysis as a function of temperature

The TGA analysis was carried out as a function of oxygen activity. The TGA measurement was started in air at room temperature and then the temperature was raised up to 1000^{o}C without changing oxygen activity. Once the temperature reached to 1000^{o}C and the weight change became a steady state, the equilibrium weight was recorded and plotted before another gas was delivered into the TGA system. The powder sample was reduced and reoxidized in a stepwise manner. The waiting periods for each equilibrium state were varied from one day to one week or more before proceeding to another oxygen activity step. The oxygen activity was decreased from 0.21 down to 1.45E-14 in step-wise at 1000^{o}C and was increased reversely up to 0.21 and then the temperature was decreased to room temperature.

The results are shown in Figures 6 and 7 (measured at 1000^{o}C). The total weight loss including the weight loss due to the temperature increase up to 1000^{o}C and PO_2 sweep is about 67 mg and the weight loss due to only PO_2 sweep from air to PO_2 = 1.45E-14 at 1000^{o}C is about 18 mg (in Figure 6). The calculated oxygen deficiencies from the weight loss from air to PO_2 = 1.45E-14 is about 0.034 moles of oxygen at 1000^{o}C. In the previous report, the oxygen occupancy (3-δ) calculated from the neutron diffraction data is 2.95 at 800^{o}C in air (in Figure 5). Even though more investigation is necessary to determine oxygen occupancy at a certain temperature, 2.95 at 800^{o}C was chosen to be the reference point based on the current data to determine the oxygen occupancies at higher than 800^{o}C. Therefore the oxygen occupancies at 1000^{o}C were estimated from the reference point at 800^{o}C from neutron diffraction (Figure 5) and the data from the TGA analysis between 800 and 1000^{o}C (Figure 3) and it was about 2.94 in air. If we use this estimation, the oxygen occupancies in PO_2 = 1.45E-14 at 1000^{o}C is 2.90 (in Figure 7). On the other hand, it was observed that the weight gain at $PO_2 = 1 \times 10^{-10}$ when PO_2 was decreased and it was not observed when PO_2 was increased. This appears to be a discrepancy in the data. More investigation about this PO_2 region is required to clarify this problem.

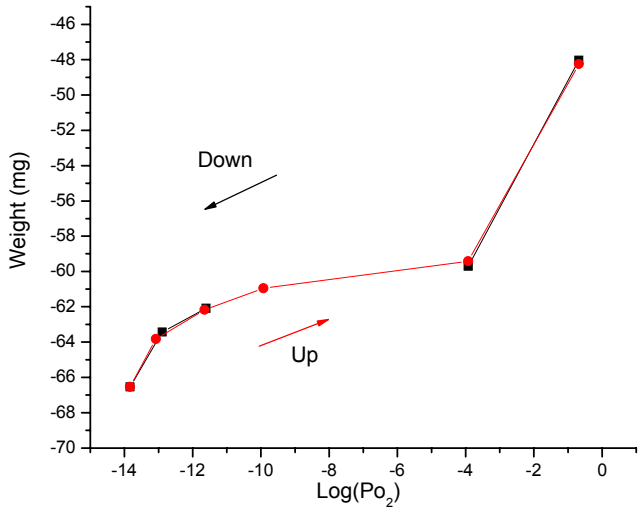

Figure 6. The weight loss of $La_{0.2}Sr_{0.8}Fe_{0.55}Ti_{0.45}O_{3-\delta}$ measured by TGA at 1000°C as a function of PO_2

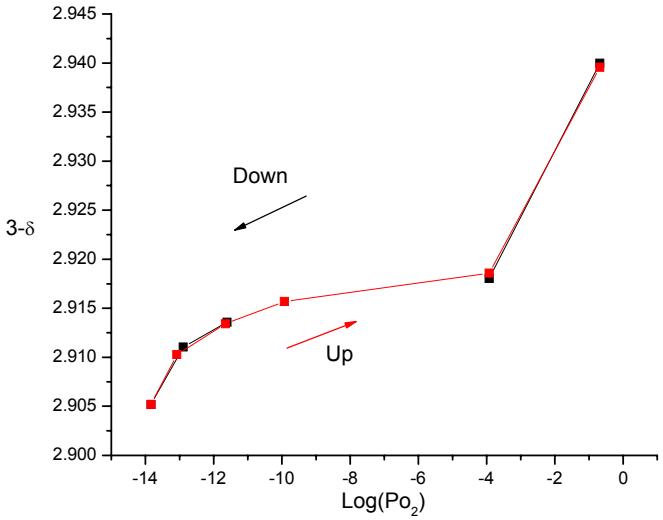

Figure 7. The oxygen occupancy of $La_{0.2}Sr_{0.8}Fe_{0.55}Ti_{0.45}O_{3-\delta}$ calculated using TGA and neutron diffraction data at 1000°C as a function of PO_2

Future studies

1. More thermogravimetric analysis on LSFT as a function of PO_2 and temperature
2. Electrical conductivity on LSFT as a function of PO_2 and temperature
3. Seebeck coefficient measurement on LSFT as a function of PO_2 and temperature

TASK 2: Determine material mechanical properties under conditions of high temperature and reactive atmosphere

Prof. S. Bandopadhyay, Dr. N. Nagabhushana and Dr. T. Nithyanantham
University of Alaska Fairbanks

In this quarter, studies were initiated on dense dual-phase OTM bar and dense LSFT samples fabricated at Praxair facility by the Co-principal investigator who spent 6 weeks at Praxair research facilities in New York.

Experimental:

LSFT ($La_{0.2}Sr_{0.8}Fe_{0.6}Ti_{0.4}O_{3-\delta}$) powder was obtained from Praxair Specialty Ceramics. The LSFT powder was prepared as dense membrane and also mixed with CGO (Ceria doped Gandolium Oxide) in the ratio of 60/40 vol%. The mixing was done by ball milling the powder in a polycarbonate vessel with Zirconia as milling media. The powders were uniaxially pressed in hardened steel die at 5000 PSI and later cold iso-statically pressed at 20KSI. The dimension of the green samples was 20 x 65 mm. The samples were sintered in air at 1400°C, for 4 hours (LSFT) and 1350°C, for 4 hours (LSFT/CGO) respectively.

Figure 8. Fully sintered and dense dual phase membranes.

Microstructure analysis of LSFT membrane:

The sintered LSFT was polished down to 3μm and thermally etched at 1350°C for 30 minutes. The etched samples were sputtered with gold for 3 minutes prior to SEM analysis.

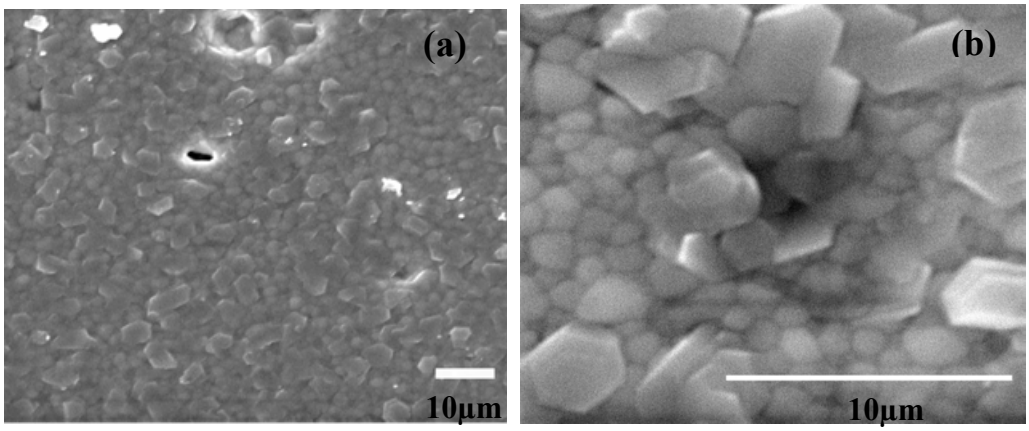

Figure 9. SEM microstructure of LSFT sintered at 1400°C. Microstructure (a) shows a densely packed grain structure and the closer observation (b) reveals the presence of two types of grains, platy hexagonal grains and closely packed fine grains.

The microstructure analysis was carried out using image analysis (Sigmascan pro 4) and the grain size distribution and average grain size were measured.

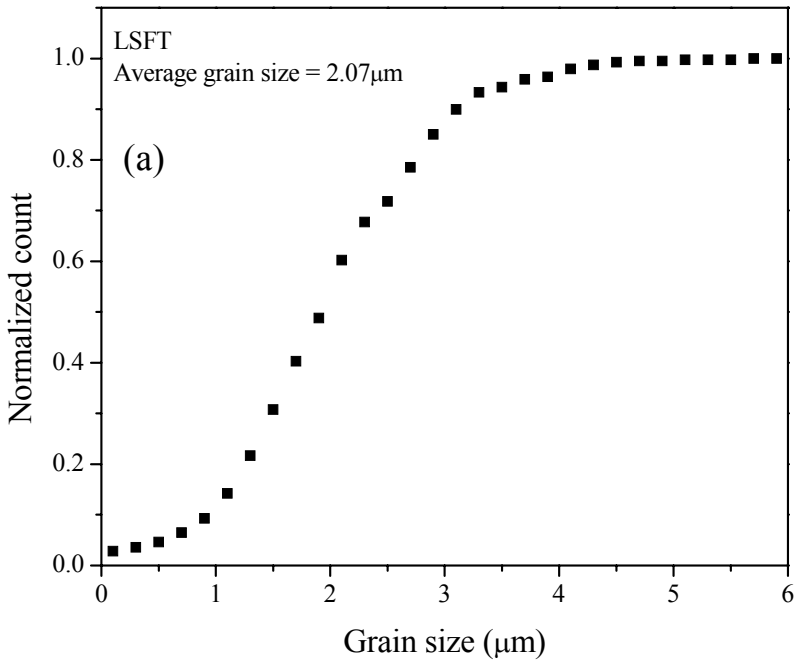

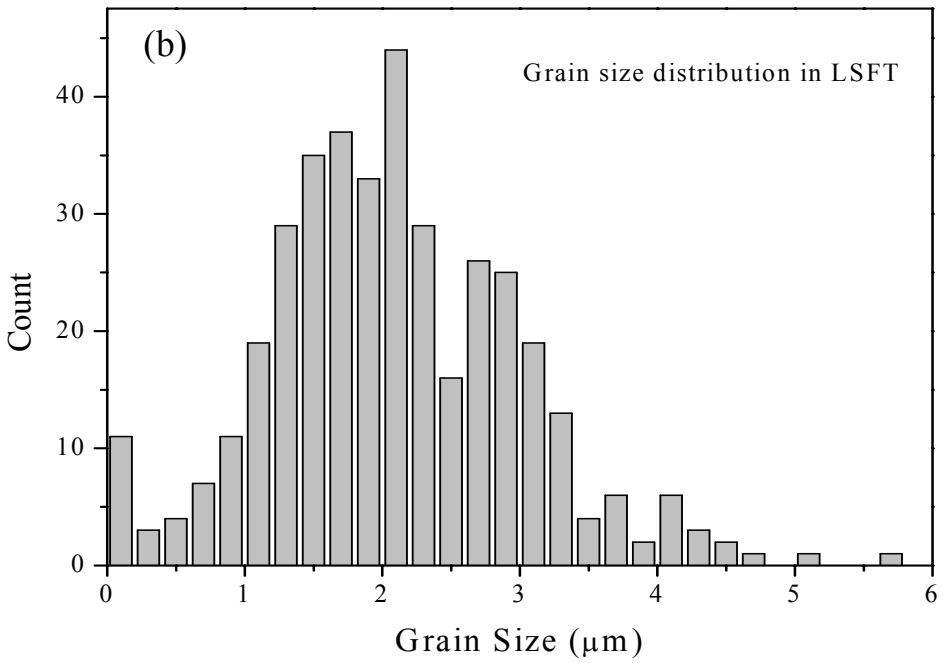

Figure 10. Grain size and distribution in sintered LSFT; (a) shows the average grain size and (b) exhibits the grain size distribution. The bimodal distribution of grains is clearly seen in the plot as well as in the microstructure.

The SEM micrograph and the image analysis showed that about 90% of the grains are less than 3.0μm with an average grain size of 2.07μm. The bimodal distribution of the grains is shown in Fig 10 (b) with a peak at 4μm.

Microstructure analysis of dual phase (LSFT/CGO) membrane:

The dual phase membrane samples were cut and ground down to 600 grade SiC paper. Further polishing of the samples did not improve polishing of the surface rather it spoiled the surface and affected the polishing. The polished samples were thermally etched and subjected to gold coating before the SEM analysis. It is evident from the micrograph that the microstructure is composed of dual phases. The dense regions are surrounded by the continuous, less dense, porous phase. It appears that the polishing led to the grain pullout from the porous region and caused deterioration of the surface. The grains pullout during fine polishing in dual phase membrane. The dense regions or phases are mostly spherical and well fused with the continuous phase. This indicates that the dense phase might be dissolving in the other phase and there is no considerable interfacial stresses developed during sintering or heat treatment. Most of the pores

are observed at the continuous phase. Composition analysis would allow identification and understanding of the chemical and crystalline nature of the phases.

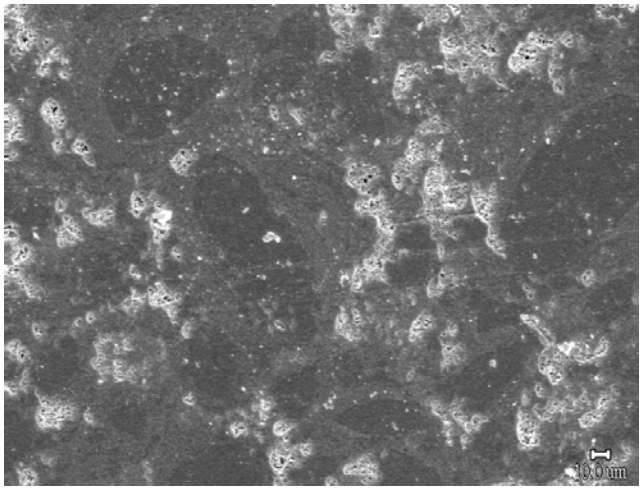

Figure 11. SEM micrograph of dual phase membrane. The dense spherical regions are enclosed by the less dense, porous, continuous phase.

The SEM micrographs of the fracture surfaces of both the materials (LSFT and dual phase) are presented in Figure 12.

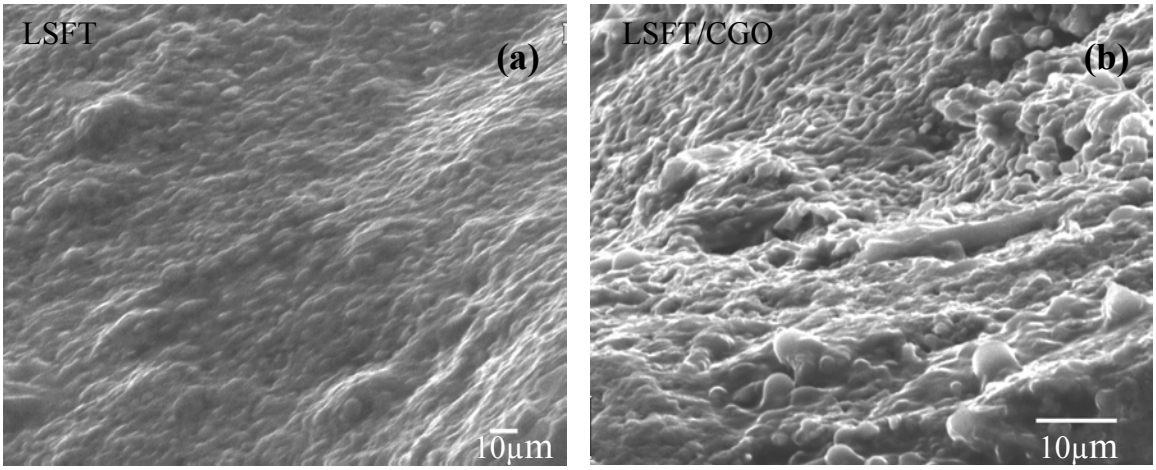

Figure 12. Fracture surfaces of the LSFT and dual phase membranes

The fracture surface of the LSFT is in accordance with the microstructure (Fig. 9) of the membrane. The fracture surface shows a densely packed grain structure and fracture mode is largely transgranular. The fracture surface of the dual phase, however, shows the presence of porous region (showed by arrow marks) and grain pullouts.

Hardness of the LSFT and dual phase membranes:

The polished samples of the membranes were used for the hardness measurement. A Vickers indenter was used for the characterization and the indentations were given at various

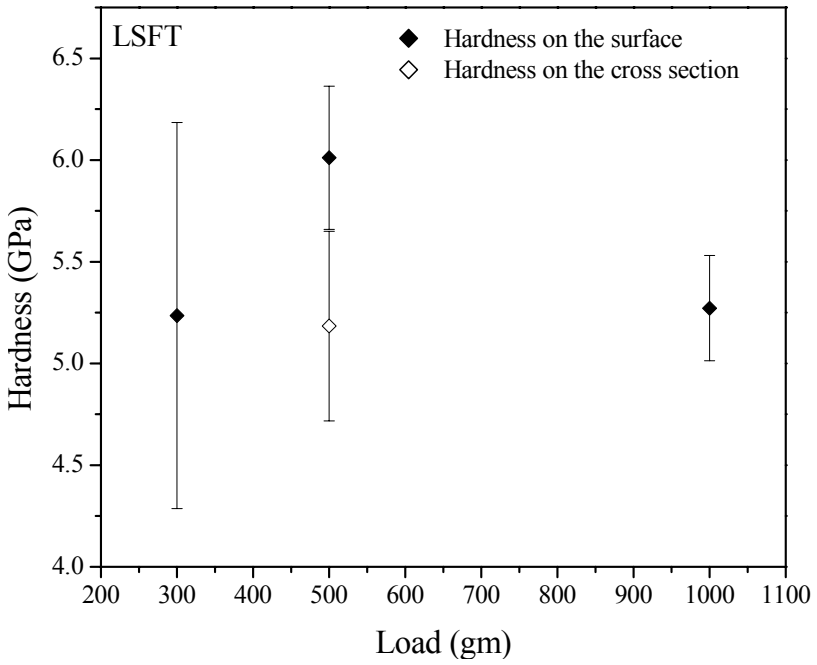

Figure 13. Hardness of the LSFT membrane

loads for 10 sec. The hardness was measured on the surface of the membrane using loads varying from 300g, 500g and 1000g respectively. The cross section of the sample was also subjected to the hardness analysis. A load of 500g was applied at various places along the cross section to study the hardness profile in the cross section. It is interesting to note the reducing scatter in the hardness values with increasing load. The indentation that formed at 300g load was very small and shallow. Hence it cannot represent the hardness of the membrane in which the pores are distributed evenly. At the load of 1000g, the indentation area is sufficiently large enough to contain the dense regions and pores together and therefore the scatter in the hardness values is relatively less.

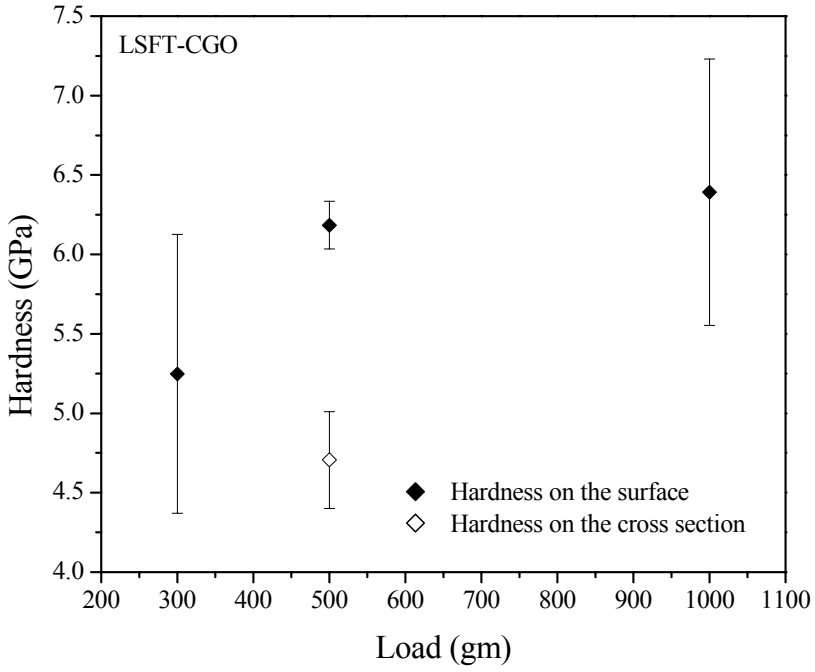

Figure 14. Hardness of the dual phase membrane.

A maximum hardness of 6.0 GPa for LSFT and 6.2 GPa for dual phase membrane were observed. In LSFT, the scatter in hardness values is decreasing with increasing load which confirms the uniform distribution of pores in the membrane. In the dual phase membrane this behavior, however, was not observed. In both the materials, in comparison the hardness at the cross section was slightly inferior than that of the surface hardness. Also there was no hardness profile along the height in the cross section.

Plans for the next quarter:

1. Extensive microstructure analysis of LSFT/CGO membranes will be done.
Dual phase membrane microstructure will be analyzed more extensively and the phase analysis will be done using SEM and XRD.

2. Effect of environment on hardness and fracture toughness of the membranes will be studied

3. Thermomechanical analysis will be initiated.

Task 3: **Measurement of Surface Activation/Reaction rates in Ion Transport Membranes using Isotope Tracer and Transient Kinetic Techniques.**

Prof. Alan Jacobson, University of Houston/University of Toronto

EXPERIMENTAL

Most of the work at UH this quarter has been directed towards completing the Seebeck measurements and further analysis of the dilatometry data. The electrochemical cell for Seebeck measurements is shown schematically in Figure 15. The top and bottom parts of the cell were composed of a pure ionic conductor, 8-wt% polycrystalline yttria-stabilized zirconia (YSZ, TZ-8Y) disc. The YSZ discs were sintered at 1450 °C for 4 h in air with a 2 °C per minute heating and cooling rate. Both sides of the YSZ disk were connected to Pt wires (0.005-inch diameter) using Pt meshes (150 × 150 mesh, 0.002-inch wire diameter, Unique Wire Weaving Co., Inc.) and Pt paste (Engelhard 6926). The top YSZ disk was used for monitoring the pO_2 and the bottom one was used for pumping the oxygen in/out of the cell. Air was used as the reference

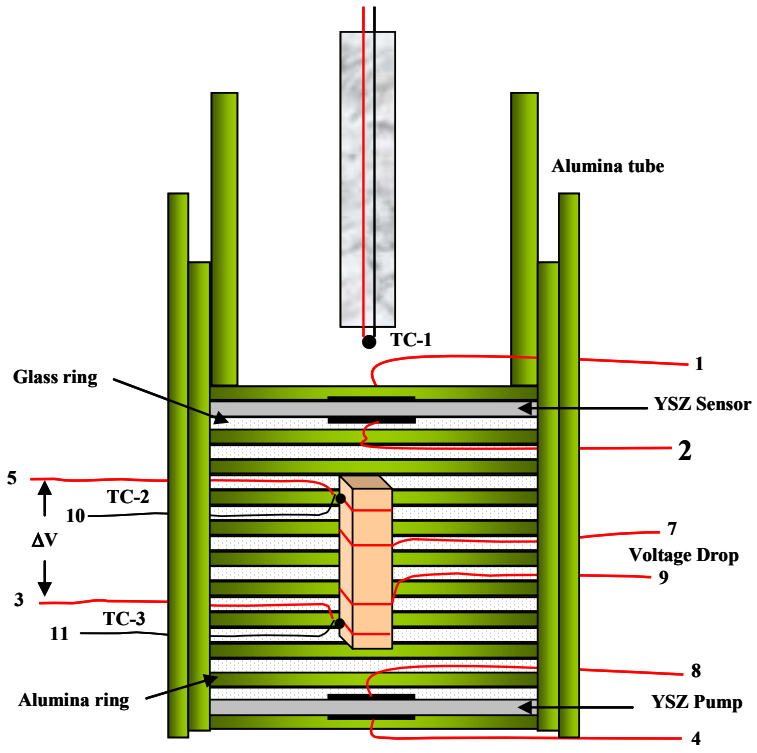

Figure 15. Electrochemical cell used for thermo-power measurements

gas. The Pt wires connected to the rectangular sample bar were brought out via the glass rings. The gas- tight seals were made by heating the cell above the softening temperature (821 °C) of the glass rings. The total height of the cell was less than 45 mm after sealing.

A rectangular bar with dimensions 0.17 × 0.18 × 1.98 cm was cut from a sample that was sintered at 1400 °C. The pump current was introduced by a 2400 SourceMeter (Keithley) and the EMF of the sensor and pump were monitored by a 2000-20 multimeter (Keithley). Three R-type thermocouples were used to monitor the temperature. One thermocouple is for the vertical furnace and other two were attached to both ends of the sample in the electrochemical cell. Cold junction compensators are connected to R-type thermocouples in order to read an accurate temperature difference. We used the natural temperature gradient along the cell. Normally this is ~ 3 °C/cm but can be varied by shifting the cell along the furnace. The EMF values between two Pt wires of the thermocouples were monitored by 2182 nano-voltameter (Keithley) with the equilibrium criteria of $\leq 5 \times 10^{-5}$ μV/min and less than a half order difference between sensor and pump pO_2.

Measurements are currently being made on LSFTO in a cell as a function of temperature and pressure at $750 \leq T \leq 1000$ °C and $\sim 10^{-17} \leq pO_2 \leq 0.3$ atm, respectively. All data points have obtained manually in order to maintain a stringent equilibrium criterion. As expected it takes more than 7 hours to obtain one data point especially in the middle of pO_2 region due to its extremely slow equilibrium kinetics.

The other experimental techniques used to generate the results reported here have been described in previous quarterly reports

RESULTS AND DISCUSSION

University of Houston

Thermopower measurements

We have continued to investigate the thermodynamic properties (stability and phase-separation behavior) and total conductivity of prototype membrane materials. The data are

needed together with the kinetic information to develop a complete model for the membrane transport. We have previously reported characterization, stoichiometry, conductivity, and dilatometry measurements for samples of $La_{0.2}Sr_{0.8}Fe_{0.55}Ti_{0.45}O_{3-x}$. In this report, we describe Seebeck data.

Measurements are being made in the cell described above as a function of temperature and pressure at $750 \leq T \leq 1000$ °C and $\sim 10^{-17} \leq pO_2 \leq 0.3$ atm, respectively. All data points have been obtained manually in order to maintain a stringent equilibrium criterion. As expected it takes more than 7 h to obtain one data point especially in the middle of pO_2 region due to the extremely slow equilibrium kinetics. The results are shown in Figure 16. The values of Seebeck coefficient increase slightly as the pO_2 decreases and then they decrease on further decrease of pO_2. The turning point of pO_2 was $\sim 2 \times 10^{-5}$ atm with $Q \sim 40.7$ μV/K at 850 °C. This behavior is frequently found in $SrFeO_{3-\delta}$ based perovskites (V. L. Kozhevnikov *et al.*, J. Solid State Chem. **158**, 320-326 (2000) and J. Mizusaki *et al.*, J. Am. Ceram. Soc. **66**, 4 247-252 (1983)). A more detailed analysis of the data will be provided in the next quarter.

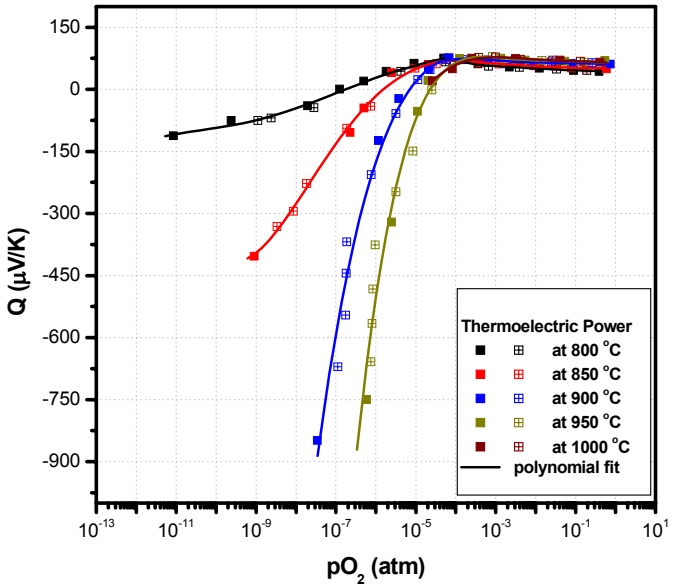

Figure 16. Thermopower results for LSFTO

Thermal Expansion Data

In this quarter, we have further analyzed the thermal analysis data reported previously. In particular we have determined the variation of the thermal expansion coefficient measured in air as a function of temperature. The results obtained by taking the derivative of dL/L with respect

to temperature are shown in Fig. 17 for the two cycles of heating and cooling (the data has been smoothed to eliminate noise in the derivative).

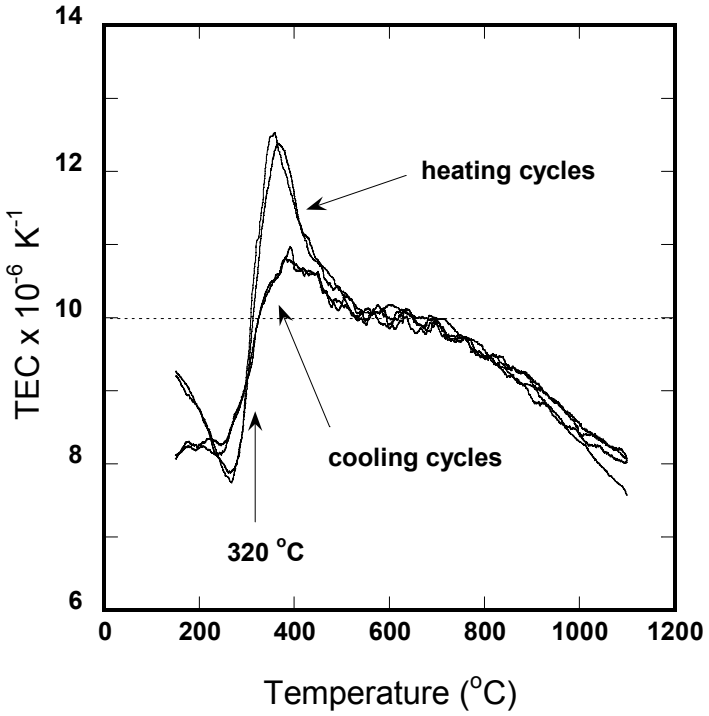

Figure 17. The variation of the total expansion coefficients of $La_{0.2}Sr_{0.8}Fe_{0.55}Ti_{0.45}O_{3-\delta}$ on heating and cooling in air at 3 °C min^{-1}.

The data are reproducible for the two heating cycles and the two cooling cycles but show some differences below 550 °C presumably due to the differences in the relative rates of oxygen loss or re-oxidation. It is interesting to note that the heating and cooling curves cross over at 320 °C, the temperature at which the kinetic of oxygen insertion or removal become limiting. On heating, the expansion coefficient reaches a maximum value of ~ 12×10^{-6} K^{-1} and then falls to ~ 10×10^{-6} K^{-1} at 550 °C. Above 750 °C, the expansion coefficient drops smoothly to ~ 8×10^{-6} K^{-1} at 1100 °C. The average TEC of $La_{0.2}Sr_{0.8}Fe_{0.55}Ti_{0.45}O_{3-\delta}$ over the whole temperature range is $9.3 \pm 1.1 \times 10^{-6}$ K^{-1}.

The chemical expansion as a function of oxygen partial pressure for $La_{0.2}Sr_{0.8}Fe_{0.55}Ti_{0.45}O_{3-\delta}$ at $790 \le T \le 956$ °C and at $\sim 10^{-15} \le pO_2 \le 0.21$ atm are shown in Fig. 18. In the high pO_2 region ($< 10^{-4}$ atm), the results agree well with the data obtained

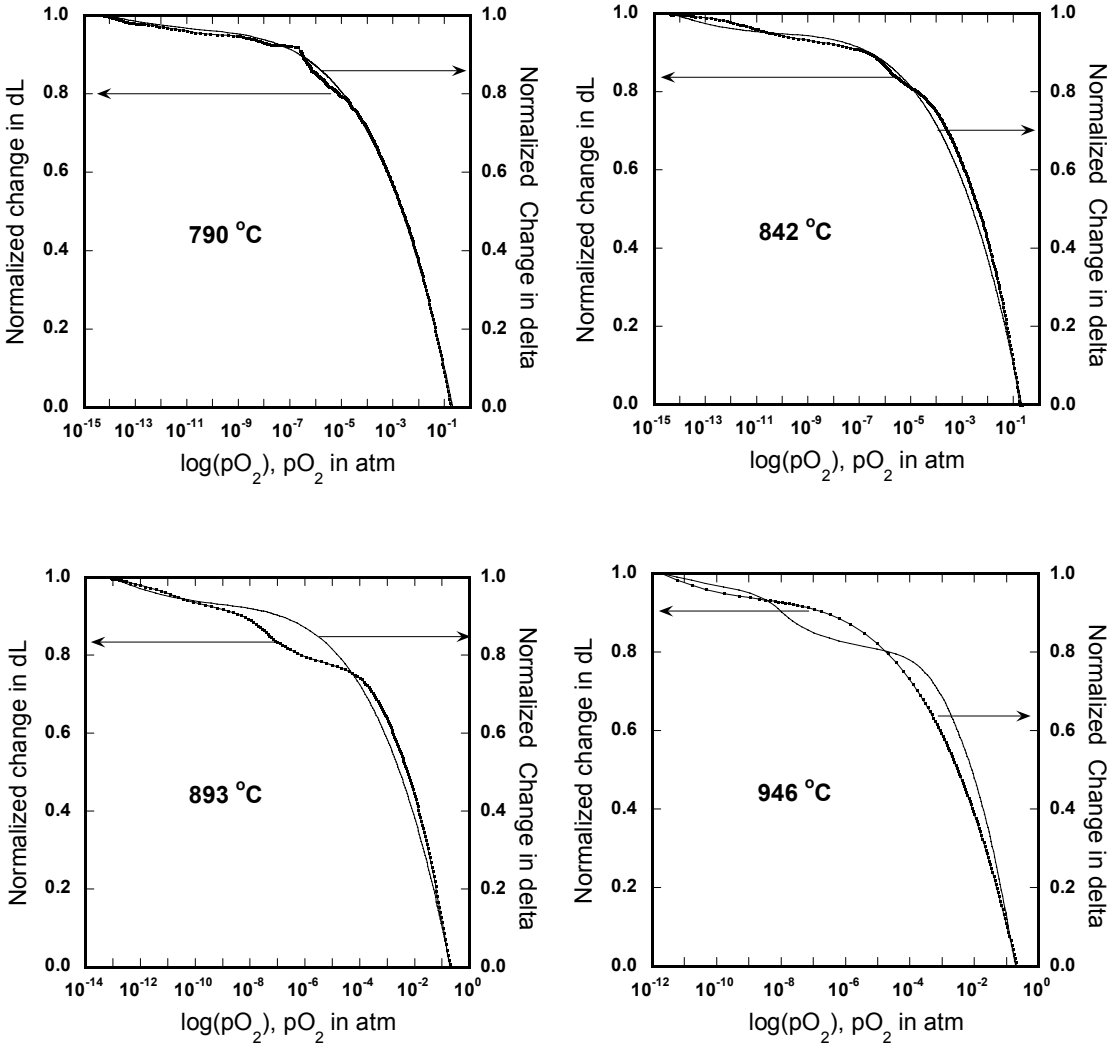

Figure 18. The chemical expansion and corresponding stoichiometry variations for $La_{0.2}Sr_{0.8}Fe_{0.55}Ti_{0.45}O_{3-\delta}$ as a function of pO_2 at four different temperatures. The data are normalized to the total change in each case.

using argon to air switches. The oxygen non-stoichiometries (δ) obtained by solid-state coulometric titration are also shown in shown in Fig. 18. Both the expansion and stoichiometry data were normalized with respect to the total change over the same pO_2 interval. The comparison shows several interesting features that were partially visible in the data below $pO_2 < 10^{-4}$ atm.

The data taken at 790 °C show a close correspondence between the variations of the chemical expansion and stoichiometry with the exception of a small deviation that begins at $pO_2 \sim 5 \times 10^{-6}$ atm. At $pO_2 < 10^{-8}$ the correlation between stoichiometry and stoichiometry is again very good. At higher temperatures the deviations become more pronounced and increase with increasing temperature. The chemical expansion initially increases faster and then plateaus at a lower pO_2 than would be predicted by the stoichiometry. The exact appearance of the correlation between stoichiometry and expansion in Figure 18 depends somewhat on the rage of pO_2 used in the normalization but the general trend is clear.

The chemical expansion data show pronounced non-equilibrium behavior in the same range of pO_2 as observed previously in conductivity measurements of LSFTO and in similar data for other ferrite compositions.

University of Toronto

Isotope Transient Studies at Steady State

As set forth in previous reports, the various surface and bulk transport parameters can be separately determined on an operating membrane by the application of an isotopic transient (a pulse of $^{18}O_2$ in our case) on one side of an operating membrane and the subsequent time dependence of ^{18}O evolution from both sides of the membrane. Both the forward and reverse surface rates can be directly measured. In flux measurements, only the net rates are available.

Summary of progress:

Air separation mode:

Our last report described progress on the analysis of the data from the isotope transients on $(La,Sr)(Fe,Cr)O_{3-x}$ LSCrF-8228. A series of measurements under low oxygen gradients (air separation mode) were analyzed. These transients were fit to the 1-D transport model, and as Figure 19 shows, the oxygen diffusivity possibly showed a mild increase of oxygen diffusivity at lower average oxygen activity. This mild variation does not cause significant variation in diffusivity across the membrane under air separation conditions. The transients could be fit with an assumed constant value of the diffusivity, a fact consistent with this expectation. Under larger gradients during syngas generation, this is no longer the case, as is seen below.

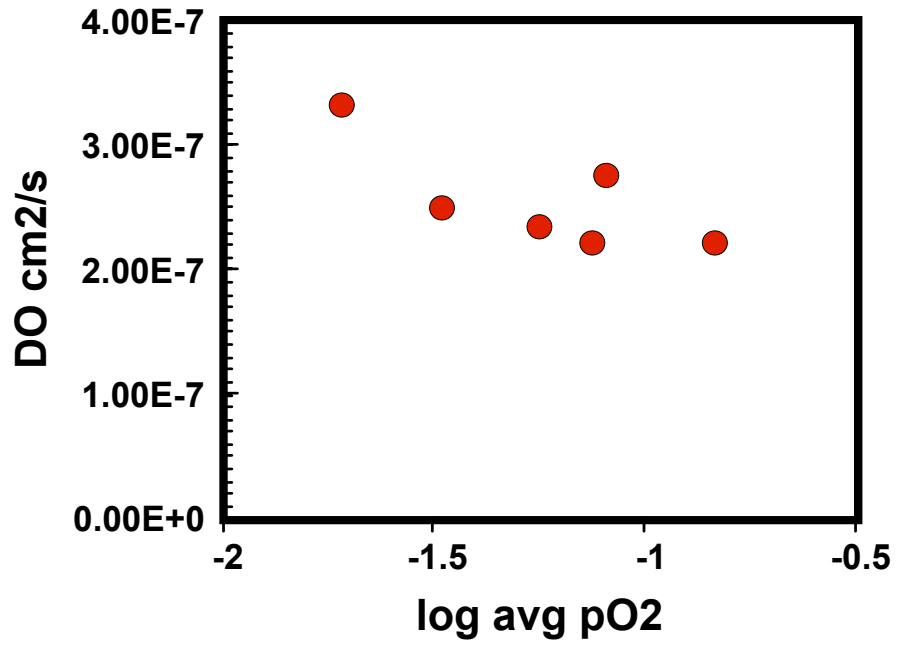

Figure 19. Oxygen diffusion coefficients, D_O , measured as a function of the average oxygen activity for the air-separation experiments.

The derived values of the forward oxygen surface activation rate coefficient for these same fits are shown in Figure 20 as a function of the air-side oxygen partial pressure, p'O_2. The main variation shows an increase in oxygen activation rate with the oxygen partial pressure in the gas phase. The cluster of points at 0.2 show some variability with the value of pO_2", the oxygen partial pressure on the delivery side. This can arise from the effect of the gradient across the membrane. A decrease in the delivery side oxygen activity decreases the effective oxygen activity at all points in the membrane, including the air-side surface. In our previous results on (La,Sr)(Fe,Co)O_{3-x} (LSCF 6482) such an effect was seen, but like the present case, the effects were too small to be unequivocally distinguished from the uncertainties in the fits. This is the case in the present data – the forward rate coefficients do not show monotonically increasing trend with oxygen activity gradient, although the highest value if k' was obtained at the largest gradient. The error estimates on these fits were obtained by trial and error fits and are similar in magnitude to the range in values of the 0.2 atm data. Under the high oxygen activity gradients of syngas generation, however, the effect of the surface condition on the surface activation rate is substantial, as seen below.

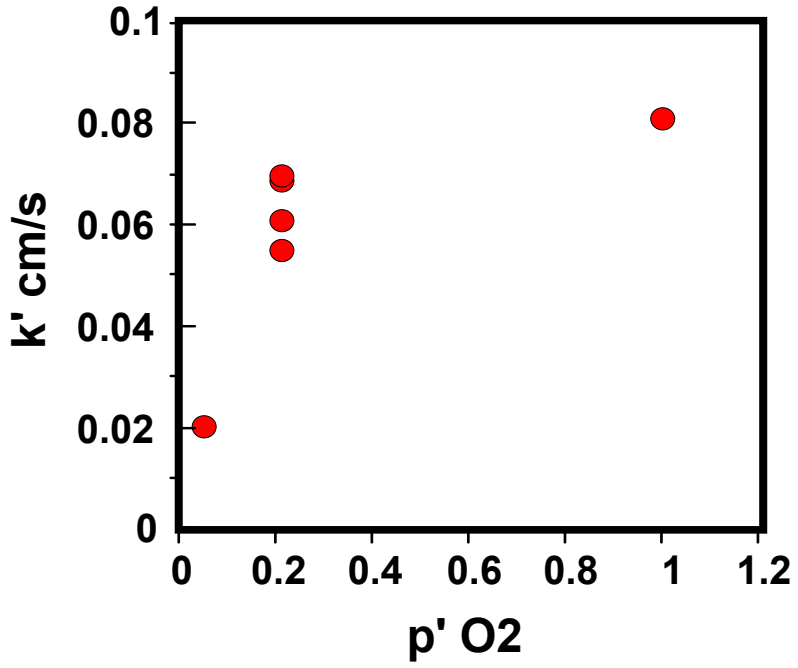

Figure 20. The forward surface activation on the air-side oxygen partial pressure, p'O_2.

High gradient experiments (CO_2/CO atmospheres on delivery side)

As discussed in the previous report, the membrane operation with a CO_2/CO on the delivery side showed two modes of operation – (1) a low flux mode where molecular oxygen is still evolved on the delivery side and (2) a high flux mode, where no oxygen is evolved, and the high rates of CO oxidation are observed. These results are reproduced in Figures 21 for the low flux condition and Figure 22 for the high flux condition. In the low flux condition, oxygen recombination was sufficiently fast to compete with CO oxidation for oxygen removal on the sweep side. This is consistent with our earlier IEDP measurements showing CO :CO_2 redox exchange rates being similar to oxygen activation on these materials. The activity gradient in the membrane was therefore modest and similar to the air separation experiments. The oxygen flux to both processes was also similar (0.21 sccm at 900 °C). The isotope composition of the CO shows that the redox exchange is not equilibrated under these conditions.

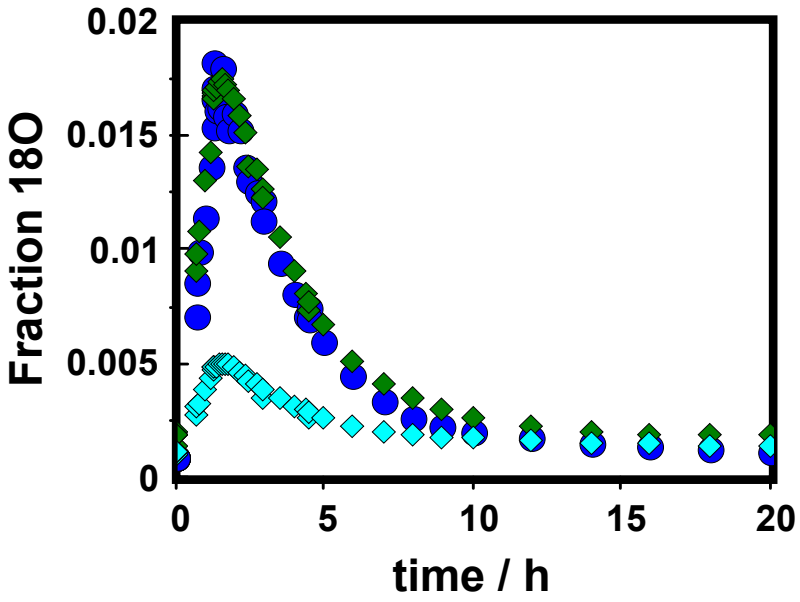

Figure 21. Isotope fraction in CO (diamonds peaking at 0.005) and in carbon dioxide (diamonds peaking at 0.02) and molecular oxygen (circles) during an isotopic transient on LSCrF 2828 membrane at 900 °C.

When the gas admitted was 50% CO, the membrane switched to high gradient – high flux mode. Figure 22 shows the isotopic transient for this experiment. The time scale is much shorter, in agreement with the substantially higher oxygen flux (2.54 sccm). Under these conditions, no molecular oxygen is seen, consistent with the delivery surface at a low oxygen potential where molecular oxygen formation is thermodynamically prohibited. Furthermore, the redox exchange between CO and CO_2 is still largely irreversible, since the isotope content in CO is lower than in carbon dioxide, which is known to be in isotopic equilibrium with the surface.

The effects of this change in gradient on the air side are consistent with the expectations in the discussions of the low gradient data. Oxygen activation was less reversible in the presence of a higher gradient, consistent with a lowering of the surface oxidation potential. This change in the surface also increased the surface forward activation rate by a factor of four. The net flux increase (by a factor of 8-10) resulted from a combination of a decrease in the reverse oxygen flux from 0.4 sccm to 0 and a simultaneous increase in the forward flux from 0.6 to 2.5. This strong effect is consistent with a higher defect density at the air surface under the higher gradient. The CO oxidation rate on the delivery side actually *increased* as the oxygen potential

on the delivery side decreased. This indicates complexities in the surface reaction mechanism on this oxide which could possibly lead to bistable behavior.

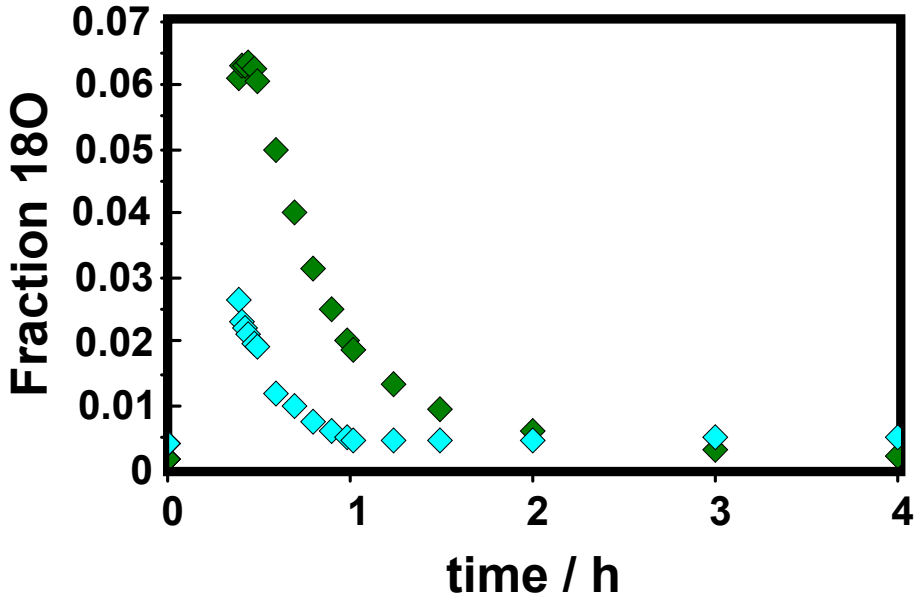

Figure 22. Isotope transient in CO (lower diamonds) and CO_2 (higher diamonds) at 900^{O}C.

The precise shape of the transient could not be fit as well with the 1-D model with a constant diffusivity as could the transients under low oxygen gradients. The best fit (constant properties) value of D_O is higher in this high gradient conditions (7 versus 2.5 x 10^{-7} cm^2/s), consistent with higher oxygen defect densities throughout the membrane. Evidence of variation in oxygen diffusivity across the membrane is also evident in the quenched profiles.

Quenched profile:

The oxygen – 18 SIMS map of the cross section of the membrane is shown in Figure 23. The schematic shows how the quenched membrane was cut for profile measurement. The cracks seen in the figure developed during the quench, and did not exist during the isotope transient. This is clear from the absence of isotopic anomalies near the cracks as have been seen in some IEDP experiments previously. An axial profile is also shown in the upper left part of the figure.

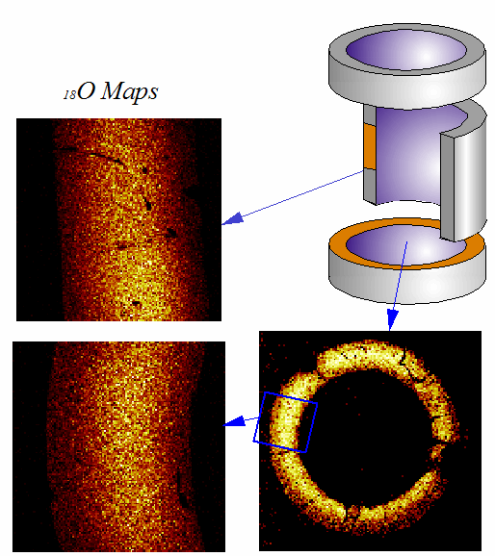

Figure 23. Quenched isotope (O-18) distribution in the LSCrF 2828 membrane. The quench was performed at 900OC under high oxygen gradient conditions as described above (see Figure 22)

The profile from the lower left (radial cut) isotope map is shown in Figure 24.

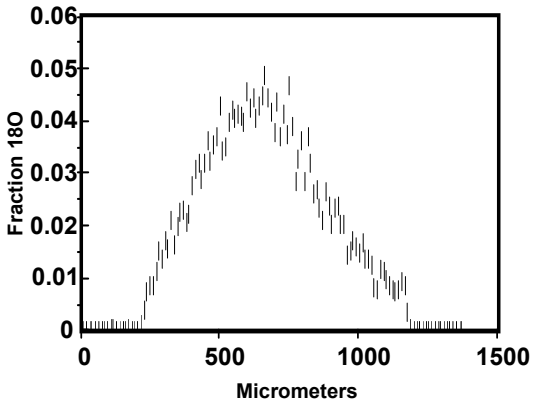

Figure 24. O-18 isotope profile for LSCrF 2828 membrane quenched during an isotope transient under high gradient conditions.

The shape of this profile is asymmetric to a degree which we cannot fit with a constant diffusivity across the membrane. The shape is consistent with a higher diffusivity near the delivery side, but complications in modeling the back-exchange of O-18 with the CO_2 require further work during the next quarter before quantitative interpretation of the data are possible.

Plans for the next quarter:

Analysis of data: Particular attention in the modelling will be paid to any resolution of the variation in D_O across the membrane in the quenched experiment.

Experimental work and improvements: Experiments on (La,Sr)(Fe,Ti)O_{3-x} membrane will be initiated. The use of GCMS will be introduced to allow us to measure small quantities of ^{18}O in CO without the interfering signal of fragmented CO_2 which arises in the online MS analysis.

Publications and Presentation:

Three abstracts have been submitted to the International Solid State Ionics conference to be held in Baden-Baden Germany July 2005. The publication of IEDP results from this program which show the ability to separate the modes of isotope exchange in CO_2, have appeared in Solid State Ionics.

CONCLUSIONS

Thermogravimetric analysis (TGA) was carried out on $La_{0.2}Sr_{0.8}Fe_{0.55}Ti_{0.45}O_{3-\delta}$ to investigate oxygen deficiency (δ) of the sample. The TGA was performed in a controlled atmosphere using oxygen, argon, carbon monoxide and carbon dioxide with adjustable gas flow rates. In this experiment, the weight loss and gain of $La_{0.2}Sr_{0.8}Fe_{0.55}Ti_{0.45}O_{3-\delta}$ was directly measured by TGA. The weight change of the sample was evaluated at between 600 and 1250^{o}C in air or 1000^{o}C as a function of oxygen partial pressure. The oxygen deficiencies calculated from TGA data as a function of oxygen activity compared well with that from neutron diffraction measurement in air. Further experimentation is needed to further clarify the effects of P_{O2} on the oxygen deficiency in the membrane.

The LSFT and LSFT/CGO membranes were fabricated at Praxair research facilities from the powder obtained from Praxair Specialty Ceramics. The sintered membranes were subjected to microstructure analysis and hardness analysis. The LSFT membrane is composed of fine grains with two kinds of grain morphology. The gain size distribution was characterized using image analysis. In LSFT/CGO membrane a lot of grain pullout was observed from the less dense, porous phase. The hardness of the LSFT and dual phase membranes were studied at various loads. The hardness values obtained from the cross section of the membranes were also compared to that of the values obtained from the surface.

A new postdoc has been hired to and joined the program in the beginning of the year. This was necessitated with the departure of the co-principal investigator Dr. N. Nagabhushana to join Praxair to work on Oxygen Transport membranes.

Further analysis of data is of vital concern for justifying many of the conclusion that could be drawn from work in the present quarter. The chemical expansion data show pronounced non-equilibrium behavior in the same range of pO_2 as observed previously in conductivity measurements of LSFTO and in similar data for other ferrite compositions. The effects of this change in gradient on the air side are consistent with the expectations in the discussions of the low gradient data. Oxygen activation was less reversible in the presence of a higher gradient, consistent with a lowering of the surface oxidation potential. This change in the surface also increased the surface forward activation rate by a factor of four. The net flux increase (by a factor of 8-10) resulted from a combination of a decrease in the reverse oxygen flux from 0.4

sccm to 0 and a simultaneous increase in the forward flux from 0.6 to 2.5. This strong effect is consistent with a higher defect density at the air surface under the higher gradient. The CO oxidation rate on the delivery side actually *increased* as the oxygen potential on the delivery side decreased. This indicates complexities in the surface reaction mechanism on this oxide which could possibly lead to bistable behavior.

REFERENCES

N/A

BIBLIOGRAPHY:

N/A

LISTS OF ACRONYMS AND ABBREVIATIONS:

OTM	Oxygen Transport Membrane
LSFCO	Lanthanum Strontium Iron Chromium Oxide ($La_{0.2}Sr_{0.8}Fe_{0.8}Cr_{0.2}O_{3-\delta}$)
LSF	Lanthanum Strontium Ferrite ($La_xSr_{1-x}FeO_{3-\delta}$)
LSCF	Lanthanum Strontium Cobalt Iron Oxide ($La_xSr_{1-x}Fe_{1-y}Co_yO_{3-\delta}$)
L2SF55T	Lanthanum Strontium Iron Titanium Oxide ($La_{0.2}Sr_{0.8}Fe_{0.55}Ti_{0.45}O_{3-\delta}$)
YSZ	Yttria stabilized zirconia
XRD	X-ray diffraction
LSFTO	$La_{0.2}Sr_{0.8}Fe_{0.55}Ti_{0.45}O_{3-\delta}$
CGO	Ceria Doped Gandolium Oxide
LSCF-6428	$La_{0.6}Sr_{0.4}Co_{0.2}Fe_{0.8}O_{3-\delta}$
LSCrF-2828	$La_{0.2}Sr_{0.8}Cr_{0.2}Fe_{0.8}O_{3-\delta}$
IEDP	Isotope exchange and depth profiling
SIMS	Secondary Ion Mass Spectroscopy